Toward Anisotropic Hybrid Materials: Directional Crystallization of Amphiphilic Polyoxazoline-Based Triblock Terpolymers

Tobias Rudolph,[†,‡] Moritz von der Lühe,[†,‡] Matthias Hartlieb,[†,‡] Sebastien Norsic,[§] Ulrich S. Schubert,[†,‡] Christophe Boisson,[§] Franck D'Agosto,[§] and Felix H. Schacher*[,†,‡]

[†]Laboratory of Organic and Macromolecular Chemistry (IOMC), Friedrich Schiller University Jena, Humboldtstraße 10, D-07743 Jena, Germany, [‡]Jena Center for Soft Matter (JCSM), Friedrich Schiller University Jena, Philosophenweg 7, D-07743 Jena, Germany, and [§]Université de Lyon, CPE Lyon, CNRS UMR 5265 Laboratoire de Chimie, Catalyse, Polymères et Procédés (C2P2), Equipe LCPP, Bat 308F, 43 Bd du 11 novembre 1918, F-69616 Villeurbanne, France

ABSTRACT We present the design and synthesis of a linear ABC triblock terpolymer for the bottom-up synthesis of anisotropic organic/inorganic hybrid materials: polyethylene-*block*-poly(2-(4-(*tert*-butoxycarbonyl)amino)butyl-2-oxazoline)-*block*-poly(2-*iso*-propyl-2-oxazoline) (PE-*b*-PBocAm0x-*b*-P*i*Pr0x). The synthesis was realized *via* the covalent linkage of azide-functionalized polyethylene and alkyne functionalized poly(2-alkyl-2-oxazoline) (POx)-based diblock copolymers exploiting copper-catalyzed azide–alkyne cycloaddition (CuAAC) chemistry. After purification of the resulting triblock terpolymer, the middle block was deprotected, resulting in a primary amine in the side chain. In the next step, solution self-assembly into core–shell-corona micelles in aqueous solution was investigated by dynamic light scattering (DLS) and transmission electron microscopy (TEM). Subsequent directional crystallization of the corona-forming block, poly(2-*iso*-propyl-2-oxazoline), led to the formation of anisotropic superstructures as demonstrated by electron microscopy (SEM and TEM). We present hypotheses concerning the aggregation mechanism as well as first promising results regarding the selective loading of individual domains within such anisotropic nanostructures with metal nanoparticles (Au, Fe_3O_4).

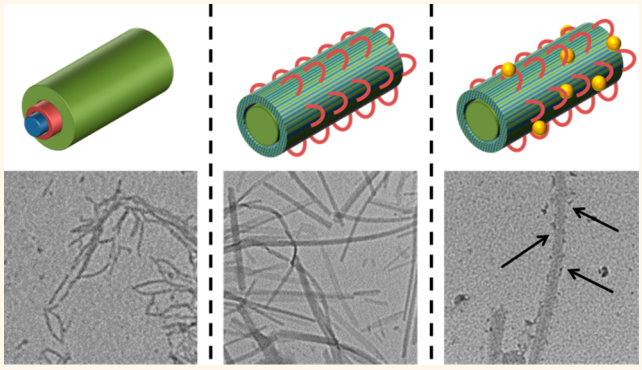

KEYWORDS: triblock terpolymer · poly(2-oxazoline)s · self-assembly · crystallization · fiber-like micelles · polyethylene

Block copolymers are an intriguing class of materials as they offer direct access to nanostructures of various morphologies and, depending on the choice of monomers, the individual blocks can be selectively functionalized. Owing to the covalent linkage between the constituting segments and the fact that most polymers are not miscible, phase separation occurs in the bulk or in selective solvents.[1−4] In both cases, size, shape, and spatial arrangement of the involved segments can be precisely controlled by the monomer sequence and the corresponding weight fractions.

If possible, block copolymers are typically synthesized *via* sequential polymerization of the respective monomers; however, for certain monomer combinations, this is not possible and alternative strategies have to be established. One elegant way is to introduce reactive end groups and use such macromolecular building blocks in suitable conjugation reactions to form block copolymers of linear or other architectures. One frequently reported example is the combination of alkyne- and azide-functionalities in copper-catalyzed azide–alkyne cycloaddition (CuAAC) reactions.[5−12] Further, the CuAAC approach has also been used for "polymerization" strategies,[13] the introduction of functional end groups,[14] the synthesis of block copolymers,[15,16] or the formation of different macromolecular architectures.[17−21] As mentioned above, block copolymers form micelles of different morphology depending

* Address correspondence to felix.schacher@uni-jena.de.

Received for review June 16, 2015 and accepted September 5, 2015.

Published online September 05, 2015
10.1021/acsnano.5b03660

on their composition, for example, spherical or cylindrical micelles. This can be induced by the introduction of selective solvents or the selective crystallization of one segment in solution.[2,22] The introduction of a crystallizable segment in block copolymers allows using directional crystallization as driving force for the formation of anisotropic nanostructures. This has been shown for ferrocenyl- and polyethylene-based materials in selective solvents.[23−27] In case of poly(ferrocenyldimethylsilane)s (PFDMS), concepts for control over micellar architecture, size, and corona compartmentalization were established by Manners and co-workers for a variety of block copolymers. Moreover, micellar size could be tuned by ultrasonication, and sequential epitaxial growth of diblock copolymer unimers as a model system for living supramolecular polymerization could be achieved. Beside cylindrical micelles, recently multidimensional superstructures of amphiphilic PFDMS-based block copolymers have been described.[28] This concept has also been extended to polyethylene containing triblock terpolymers by Schmalz and co-workers.[26] In this context, another interesting semicrystalline polymer is poly(2-*iso*-propyl-2-oxazoline) (P*i*PrOx), which shows directional growth into fiber-like structures upon heating above the LCST in aqueous media.[29−32] With the use of cationic ring-opening polymerization (CROP), P*i*PrOx can easily be combined with functional end-groups or blocks enabling various functionalization strategies.[33] The incorporation of amine containing oxazolines can be used to increase the affinity toward incorporation of metal ions like described for other amine-functionalized polymers.[34,35]

Complexation of metals in polymer nanostructures leads to the formation of new hybrid materials, which often combine the physical properties of the polymer and inorganic materials.[36−38] Beside the direct incorporation of metal ions into monomers like in case of PFDMS-based materials, certain polymers have the ability to attract or stabilize metal nanoparticles.[39,40] Typically, polyelectrolytes such as poly(ethylenimine) (PEI),[41] poly(acrylic acid) (PAA),[42] or nonionic materials featuring nitrogen or oxygen atoms along the polymer chains are used.[40] The combination of both approaches, *i.e.*, the formation of anisotropic superstructures by directed crystallization and the access to organic/inorganic hybrid materials *via* complexation of metal nanoparticles within block copolymer nanostructures, is particularly attractive. In that way, the synthesis of anisotropic hybrid materials with feature sizes typically not accessible by top-down approaches can be realized and prospective applications in nanoelectronics or as biochemical and optical sensors can be envisioned.[43−45]

Herein, we demonstrate the synthesis of polyethylene-*block*-poly(2-(4-(*tert*-butoxycarbonyl)-amino)butyl-2-oxazoline)-*block*-poly(2-*iso*-propyl-2-oxazoline) (PE-*b*-PBocAmOx-*b*-*i*PrOx) using a combination of catalytic olefin polymerization, cationic ring-opening polymerization (CROP), and copper-catalyzed azide−alkyne cycloaddition (CuAAC). The middle block, PBocAmOx, can be selectively deprotected, introducing a primary amine in the side chain (PAmOx). In the next step, we investigated the solution self-assembly in selective solvents and demonstrate the formation of core−shell−corona micelles by dynamic light scattering (DLS) and transmission electron microscopy (TEM). Subsequently, directional crystallization of the corona-forming block, poly(2-*iso*-propyl-2-oxazoline), can be used to form anisotropic superstructures of the initial spherical building blocks. Depending on whether PBocAmOx or PAmOx forms the middle segments, differences in the self-assembly mechanism or the resulting morphologies are highlighted. Further, selective introduction of gold and iron oxide nanoparticles into the PAmOx domain shows the potential of the herein demonstrated approach for the formation of extended hybrid nanowires.

RESULTS AND DISCUSSION

To create anisotropic nanostructures, which can then be selectively loaded using metal ions or metal nanoparticles, a two-step approach for the solution self-assembly of triblock terpolymers was utilized. For this, we designed a polyethylene-*block*-poly(2-(4-(*tert*-butoxycarbonyl)amino)butyl-2-oxazoline)-*block*-poly(2-*iso*-propyl-2-oxazoline) (PE-*b*-PBocAmOx-*b*-P*i*PrOx) triblock terpolymer (Scheme 1). In a first step, self-assembly in water as selective solvent leads to the formation of core−shell−corona micelles with a PE core, a PBocAmOx shell and a P*i*PrOx corona. Subsequent heating above the LCST of P*i*PrOx is then supposed to induce directional crystallization and the formation of anisotropic superstructures. Such directional crystallization processes might serve as key technique for the formation of compartmentalized hybrid structures or the precise design of polymer−polymer or polymer−metal interfaces. The middle block, PBocAmOx, can be transformed into poly(2-(4-amino)butyl-2-oxazoline) (PAmOx) and used for the complexation of metal ions afterward. For the synthesis of PE-*b*-PBocAmOx-*b*-P*i*PrOx, we used an azide-functionalized PE in combination with alkyne-functionalized PBocAmOx-*block*-PiPrOx diblock copolymers in copper-catalyzed azide−alkyne cycloaddition (CuAAC) reactions.

Synthesis of Azide Functionalized Polyethylene (PE−N_3). Azide-functionalized polyethylene (PE_{36}−N_3, the subscript denotes the degree of polymerization) was synthesized *via* a catalyzed polyethylene chain growth on magnesium leading to *n*-dipolyethylenylmagnesium compounds that are deactivated by iodine. The resulting iodo end-functionalized polyethylene chains (PE−I) are transformed into an azide end-functionalized PE (PE−N_3) using sodium azide (Scheme S1).[46−48] PE_{36}−N_3 was characterized by nuclear magnetic

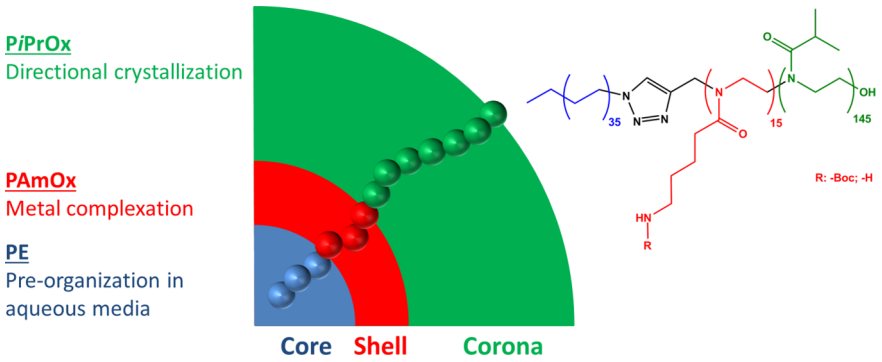

Scheme 1. Illustration of the designed PE-*b*-PBocAmOx-*b*-P*i*PrOx triblock terpolymer and a brief description of the purpose of each block.

resonance spectroscopy (NMR), high temperature size exclusion chromatography (HT-SEC), and FT-IR (Figures S1−S3). The degree of functionalization for PE−N_3 is in the range of 87%, while the molar mass (M_n) was determined *via* NMR to be 1060 g mol^{-1} (Figure S2). The latter was determined by comparing the integrals of the terminal methyl group and the backbone. The remaining 13% PE can be assumed to consist of fully aliphatic and vinyl-terminated PE. The characteristic azide peak at 2094 cm^{-1}, as well as CH_2 vibrations between 3000−2800 cm^{-1}, were found by FT-IR (Figure S3).

Synthesis of an Alkyne-Functionalized TB-PBocAmOx-*b*-P*i*PrOx Diblock Copolymer. The synthesis of the alkyne-functionalized poly(2-alkyl-2-oxazoline) counterpart was realized *via* sequential CROP of 2-(4-(*tert*-butoxycarbonyl)amino)-butyl-2-oxazoline (BocAmOx)[49] and 2-*iso*-propyl-2-oxazoline (*i*PrOx) using established microwave-assisted techniques. For the introduction of an alkyne functionality, propargyl *p*-toluenesulfonate (TB-Ts) was used as initiator in acetonitrile (CH_3CN) at 140 °C. BocAmOx was polymerized at a concentration of 1 mol L^{-1} and a monomer to initiator ratio ([M]/[I]) of 15 (Scheme S2). Afterward, an *i*PrOx stock solution (in CH_3CN, [M]/[I] = 150) was added to the polymerization mixture (1 mol L^{-1}), and again placed in the microwave synthesizer at 140 °C. The polymerization was stopped by the addition of water, followed by precipitation in diethyl ether. The obtained materials were characterized *via* NMR, SEC, and FT-IR (Figure 1; Figures S4−S6). The degree of polymerization (DP) of the precursor (TB-PBocAmOx) was determined *via* NMR by integration of the aromatic signals of the tosylate and the signals corresponding to the repeating unit, confirming a DP of 15. For the block extension, SEC shows a shift of the elution trace, without any signs of remaining homopolymer (Figure S4). The composition of the block copolymer was determined in comparison to the characteristic BocAmOx signals in NMR, leading to TB-PBocAmOx$_{15}$-*b*-P*i*PrOx$_{145}$ (TB refers to the introduced triple bond as starting group). The degree of polymerization for the second block is slightly lower compared to the [M]/[I] ratio of 150, which is attributed to incomplete

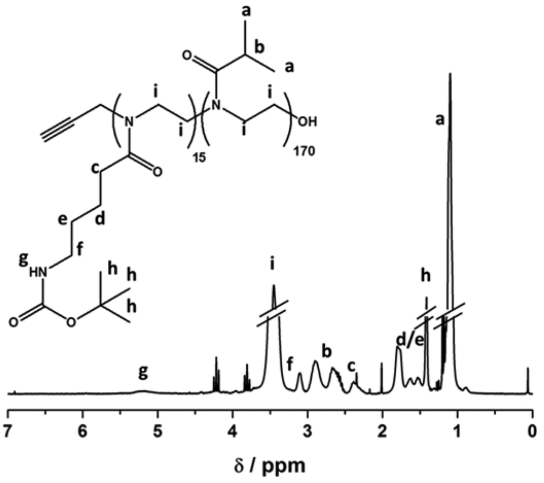

Figure 1. ^{1}H NMR spectrum for TB-PBocAmOx$_{15}$-*b*-P*i*PrOx$_{145}$ and peak assignment (300 MHz; $CDCl_3$).

monomer conversion as observed *via* NMR (Figure S5). Further, the block copolymer was investigated *via* FT-IR, showing signals for the amide at 3300 cm^{-1}, for the carbonyl of the protective group at 1705 cm^{-1}, for the amide at 1516 cm^{-1}, and an increase in the region of methyl groups (1365 cm^{-1}; Figure S6).

CuAAC Reaction Between PE$_{36}$−N_3 and TB-PBocAmOx$_{15}$-*b*-P*i*PrOx$_{145}$. For the copper-catalyzed azide−alkyne cycloaddition (CuAAC) reaction between PE$_{36}$−N_3 and TB-PBocAmOx$_{15}$-*b*-P*i*PrOx$_{145}$, both components were dissolved in THF at 120 °C in a sealed pressure vial (Figure 2A). PE$_{36}$−N_3 was added in a 3-fold excess to ensure full conversion of the alkyne functionalities. The solution was degassed with argon, and *N*,*N*,*N*′,*N*″,*N*″-pentamethyldiethylenetriamine (PMDETA; 2 equiv) and copper bromide (CuBr; 2 equiv) were added under argon flux. The sealed vial was heated for 1 h at 120 °C as we suppose that at this temperature PE is molten to a great extent (Figure S7), and a clear green solution was observed. Afterward, the reaction was allowed to cool to room temperature (RT), diluted with dichloromethane (CH_2Cl_2) and mixed with water. The aqueous solution turned blue due to the presence of Cu^{2+}, while the organic phase was clear. The organic phase was

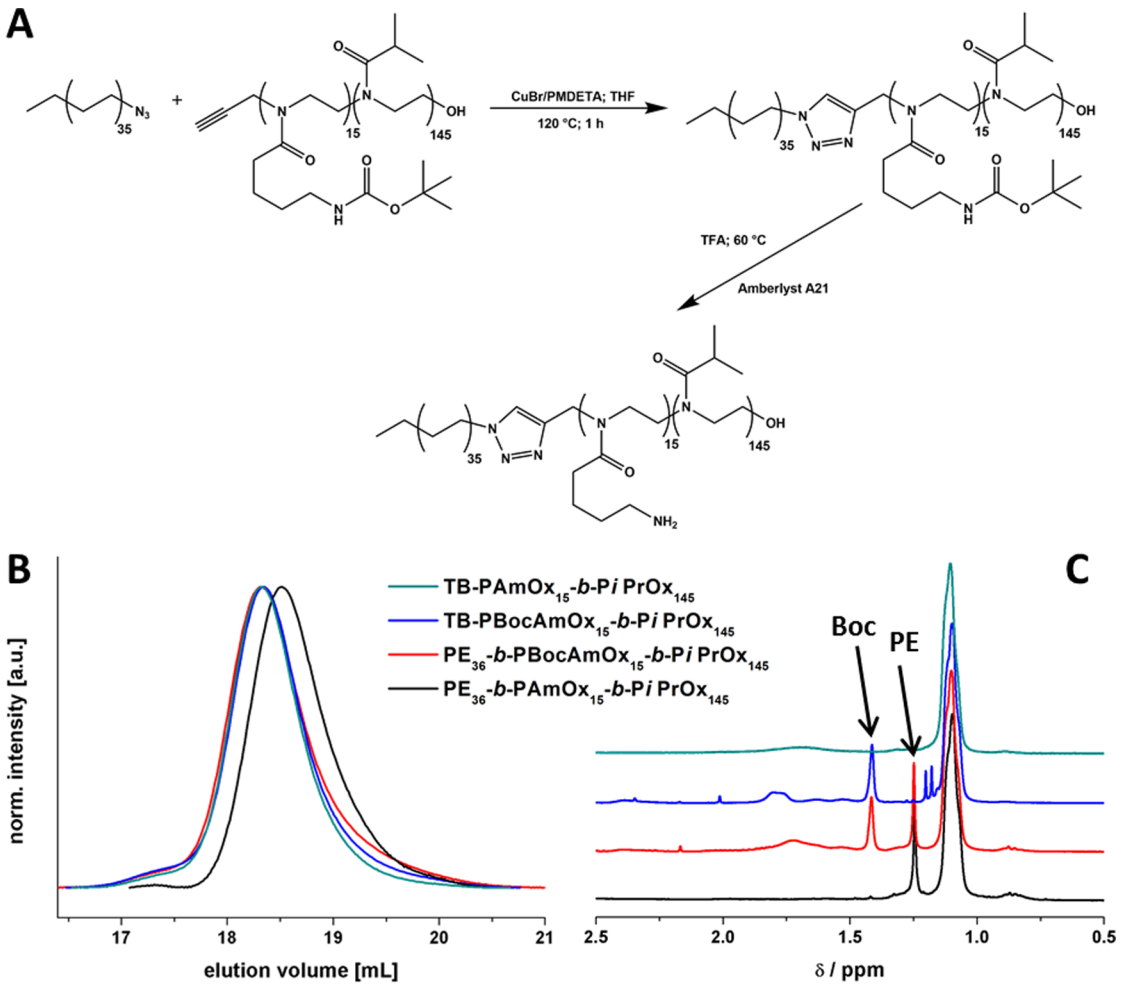

Figure 2. (A) CuAAC cycloaddition reaction between $PE_{36}-N_3$ and TB-$PBocAmOx_{15}$-*b*-P*i*$PrOx_{145}$ toward PE_{36}-*b*-$PBocAmOx_{15}$-*b*-P*i*$PrOx_{145}$; sequential deprotection of the Boc group under acidic conditions; (B) comparison of SEC traces for TB-$PBocAmOx_{15}$-*b*-P*i*$PrOx_{145}$ (cyan curve), TB-$PAmOx_{15}$-*b*-P*i*$PrOx_{145}$ (blue curve), PE_{36}-*b*-$PBocAmOx_{15}$-*b*-P*i*$PrOx_{145}$ (red curve), and PE_{36}-*b*-$PAmOx_{15}$-*b*-P*i*$PrOx_{145}$ (black curve); (C) comparison of ^{1}H NMR spectra for TB-$PBocAmOx_{15}$-*b*-P*i*$PrOx_{145}$ (cyan curve), TB-$PAmOx_{15}$-*b*-P*i*$PrOx_{145}$ (blue curve), PE_{36}-*b*-$PBocAmOx_{15}$-*b*-P*i*$PrOx_{145}$ (red curve), and PE_{36}-*b*-$PAmOx_{15}$-*b*-P*i*$PrOx_{145}$ (black curve).

removed, filtered twice using syringe filters (PTFE, 0.45 μm), and precipitated into diethyl ether. The excess of $PE-N_3$ forms large aggregates and was removed by filtration, while the generated triblock terpolymer is well soluble due to the high poly(2-alkyl-2-oxazoline) (POx) content. The resulting triblock terpolymer was investigated *via* FT-IR, NMR and SEC. With the use of FT-IR, the disappearance of the azide peak (2094 cm^{-1}) was observed and new signals at 2916 and 2846 cm^{-1} corresponding to PE appear (Figures S8 and S9). With the use of ^{1}H NMR, the triblock terpolymer shows a new signal at 1.25 ppm, again corresponding to the methylene protons of the main PE chain, whereas the comparison with signals for the POx backbone (around 3.6 ppm) indicates an equimolar incorporation of PE (Figure S10). This was used for the determination of the composition, yielding the triblock terpolymer PE_{36}-*b*-$PBocAmOx_{15}$-*b*-P*i*$PrOx_{145}$ (Figure 2C; Figure S11). Due to interactions of PBocAmOx and the column material of the HT-SEC used, it was not possible to study these materials by this technique. SEC of PE_{36}-*b*-$PBocAmOx_{15}$-*b*-P*i*$PrOx_{145}$ was performed using either dimethylacetamide (DMAC) or chloroform ($CHCl_3$) as eluent. In both cases, the SEC traces show comparable molar masses as observed for TB-$PBocAmOx_{15}$-*b*-P*i*$PrOx_{145}$ (Table 1; Figure 2B). Nevertheless, we assume this to result from the rather low DP of the $PE_{36}-N_3$ segment. No characteristic trapezoid aggregates as reported for the crystallization of PE were found in TEM studies (see also Figure S12). We therefore assume that contamination of the samples with unreacted PE_{36}-N_3 is negligible.[50]

In the next step, the deprotection of TB-$PBocAmOx_{15}$-*b*-P*i*$PrOx_{145}$ and PE_{36}-*b*-$PBocAmOx_{15}$-*b*-P*i*$PrOx_{145}$ was performed using trifluoroacetic acid (TFA, Figure 2A). After purification using an Amberlyst resin, the resulting materials revealed no differences by SEC for $PAmOx_{15}$-*b*-P*i*$PrOx_{145}$, while in case of PE_{36}-*b*-$PAmOx_{15}$-*b*-P*i*$PrOx_{145}$, a shift to higher elution volume in comparison to PE_{36}-*b*-$PBocAmOx_{15}$-*b*-P*i*$PrOx_{145}$ was found

TABLE 1. Characterization of the Herein Used Homopolymers, Diblock Copolymers, and Triblock Terpolymers

polymer	M_n [g mol^{-1}][a]	M_n [g mol^{-1}][b]	Đ[b]	M_n [g mol^{-1}][c]	Đ[c]	ratio hydrophilic/hydrophobic [wt %/wt %]
PE_{36}—N_3	1060	1290[d]	1.16[d]	-		—/100
TB-PBocAmOx$_{15}$-*b*-P*i*PrOx$_{145}$	20000	23500	1.08	28000	1.09	82/18
TB-PAmOx$_{15}$-*b*-P*i*PrOx$_{145}$	18500	-[e]	-[e]	29000	1.07	100/—
PE_{36}-*b*-PBocAmOx$_{15}$-*b*-P*i*PrOx$_{145}$	21000	24000	1.09	27000	1.11	78/22
PE_{36}-*b*-PAmOx$_{15}$-*b*-P*i*PrOx$_{145}$	19500	-[e]	-[e]	25000	1.06	95/5

[a] Calculated from NMR. [b] SEC ($CHCl_3$/*i*-PrOH/TEA) (PS-calibration). [c] SEC (DMAC/LiCl) (PS-calibration). [d] HT-SEC (TCB at 150 °C) (PE-calibration). [e] Not determined due to interactions with the column material.

(Figure 2B). Both NMR and FT-IR confirmed the successful deprotection through disappearance of the characteristic signals for the Boc-group (Figure 2C; Figures S13—S16). FT-IR measurements indicated the presence of small amounts of residual TFA after deprotection due to signals in the range of 1700—1800 cm^{-1}. Additional signals corresponding to the free amine can be observed in the fingerprint region (Figures S15 and S16). All important characteristics for PE_{36}-*b*-PAmOx$_{15}$-*b*-P*i*PrOx$_{145}$, PE_{36}-*b*-PBocAmOx$_{15}$-*b*-P*i*PrOx$_{145}$, TB-PBocAmOx$_{15}$-*b*-P*i*PrOx$_{145}$ and PAmOx$_{15}$-*b*-P*i*PrOx$_{145}$, including the respective hydrophilic to hydrophobic ratio, are summarized in Table 1.

Solution Behavior in Water As Selective Solvent. We were now interested in the solution behavior of the materials in aqueous solution. Therefore, the materials were dissolved in a nonselective solvent, dimethylformamide (DMF), and heated for 10 min at 120 °C at a concentration of 1 mg mL^{-1}; under these conditions, we assume the triblock terpolymers exist as unimers as the PE block is within its melting range (Figure S7). After the samples had cooled to room temperature, the solutions were investigated *via* DLS, already indicating the formation of micelles with a hydrodynamic radius of $\langle R_h \rangle_{n,app}$ = 8 nm (in DMF; Figure S17), and afterward were dialyzed against water for 2 days (RC MWCO 1000 Da) to remove any remaining DMF. We now anticipate the formation of core—shell-corona micelles featuring a PE core, a PBocAmOx or PAmOx shell, and a P*i*PrOx corona (Figure 3A). Both corresponding diblock copolymers could be directly dissolved in water, although micelles are formed immediately in case of TB-PBocAmOx$_{15}$-*b*-P*i*PrOx$_{145}$. The resulting solutions were investigated *via* dynamic light scattering (DLS), transmission electron microscopy (TEM) and zeta-potential measurements. The hydrodynamic radius (R_h) according to DLS varies, depending on the terpolymer composition. Micelles with hydrodynamic radii of 17 nm (PE_{36}-*b*-PBocAmOx$_{15}$-*b*-P*i*PrOx$_{145}$) and 14 nm (PE_{36}-*b*-PAmOx$_{15}$-*b*-P*i*PrOx$_{145}$) were found (Figure 3B). While PAmOx$_{15}$-*b*-P*i*PrOx$_{145}$ can be regarded as double hydrophilic and unimers with a R_h of 2 nm are found, TB-PBocAmOx$_{15}$-*b*-P*i*PrOx$_{145}$ forms core—corona micelles with a R_h of 13 nm, where the core is formed by PBocAmOx and the corona consists of P*i*PrOx. TEM confirms the spherical shape of the core—shell-corona micelles in aqueous solution (Figure 3C). With zeta-potential measurements, a value of −0.5 mV was found for PE_{36}-*b*-PBocAmOx$_{15}$-*b*-P*i*PrOx$_{145}$, while a slightly positive value of +8.5 mV was obtained for PE_{36}-*b*-PAmOx$_{15}$-*b*-P*i*PrOx$_{145}$ micelles (at pH 7), indicating the presence of protonated primary amine groups.

Directional Crystallization of P*i*PrOx. The crystallization of P*i*PrOx from aqueous solution upon heating above the cloud point temperature at 65 °C has been reported by Schlaad and co-workers. They proposed a combination of nonspecific hydrophobic interactions and oriented dipolar interactions as main driving force.[29] Also, recent efforts by Dworak *et al.* have shown that P*i*PrOx crystallization can be achieved in organic media such as acetonitrile or dimethyl sulfoxide as well.[51] Our aim was to use the previously described core—shell—corona micelles with a P*i*PrOx corona as building blocks during directional crystallization,[29—31,52] as also recently conceptually demonstrated for double crystalline block copolymers, PFDMS-*b*-P*i*PrOx.[53] Initial investigations at concentrations of up to 20 mg mL^{-1} resulted in rather rapid formation of a macroscopic precipitate, and we therefore decreased the concentration to values between 0.33 and 0.1 mg mL^{-1} for all following investigations. The aqueous copolymer solutions were heated for 24 h at 65 °C, and the scattering intensity of the micellar solutions was monitored by DLS (Figure 4). In all cases, the overall scattering intensity strongly increased within 1 min, as 65 °C exceeds the cloud point temperature (T_{cp}) of P*i*PrOx. Afterward, a further slight increase can be observed, followed by a sharp drop after 10—12 h in case of PE_{36}-*b*-PAmOx$_{15}$-*b*-P*i*PrOx$_{145}$, while only a slight decrease can be seen for PE_{36}-*b*-PBocAmOx$_{15}$-*b*-P*i*PrOx$_{145}$ (Figure 4). The corresponding hydrodynamic radii for PE_{36}-*b*-PAmOx$_{15}$-*b*-P*i*PrOx$_{145}$ constantly increase until the respective correlation function shows more than one mode, leading to the assumption that two different aggregate populations coexist (Figure S18). Presumably, the P*i*PrOx chains initially collapse and form larger aggregates, which then start to crystallize until precipitation occurs. One possible explanation is that the rather low degree of polymerization of PAmOx in combination with steric constraints due to chain folding decreases the stabilization of these structures. This observation has also been reported for linear

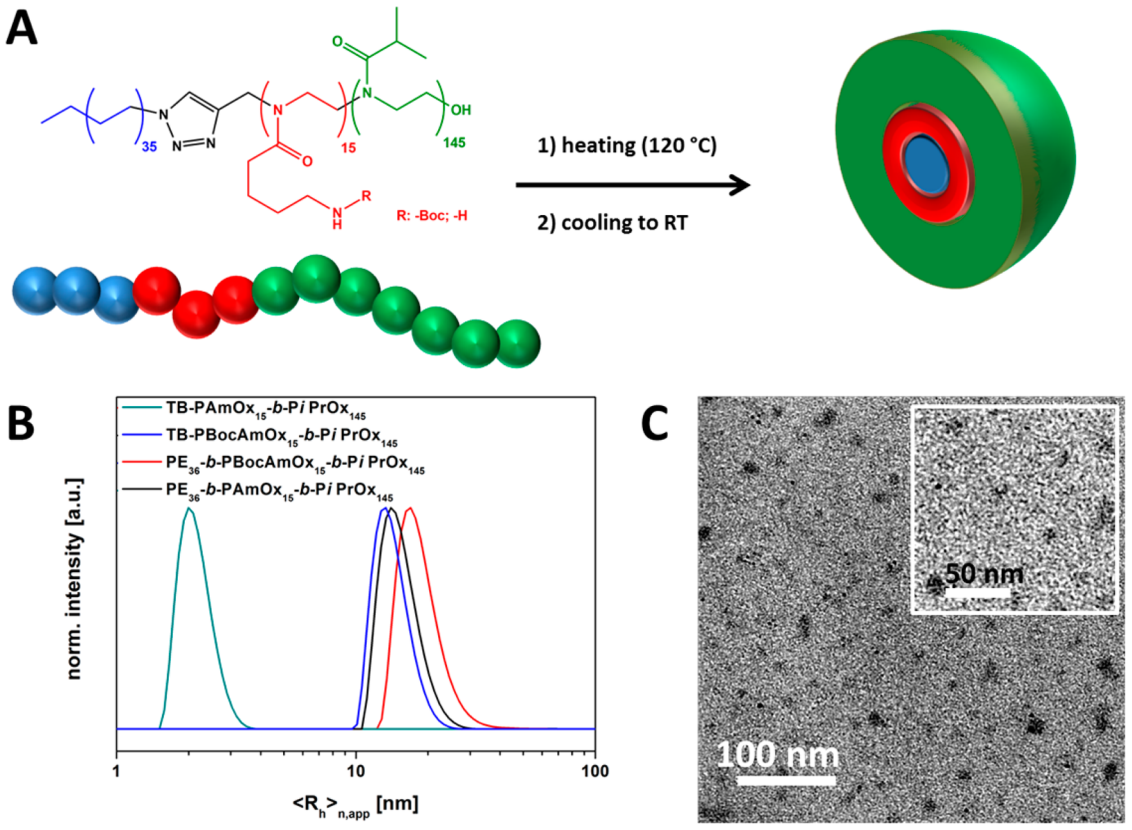

Figure 3. (A) Illustration of micelle formation of PE_{36}-*b*-$PAmOx_{15}$-*b*-P*i*$PrOx_{145}$ or PE_{36}-*b*-$PBocAmOx_{15}$-*b*-P*i*$PrOx_{145}$ after heating and cooling in DMF; (B) comparison of DLS size distributions for TB-$PBocAmOx_{15}$-*b*-P*i*$PrOx_{145}$ (blue curve; $\langle R_h \rangle$ = 2 nm), TB-$PAmOx_{15}$-*b*-P*i*$PrOx_{145}$ (cyan curve; $\langle R_h \rangle$ = 13 nm), PE_{36}-*b*-$PBocAmOx_{15}$-*b*-P*i*$PrOx_{145}$ (red curve; $\langle R_h \rangle$ = 17 nm), and PE_{36}-*b*-$PAmOx_{15}$-*b*-P*i*$PrOx_{145}$ (black curve; $\langle R_h \rangle$ = 14 nm); (C) TEM micrograph for PE_{36}-*b*-$PAmOx_{15}$-*b*-P*i*$PrOx_{145}$ micelles in water (0.33 mg mL^{-1}); the inset shows a higher magnification.

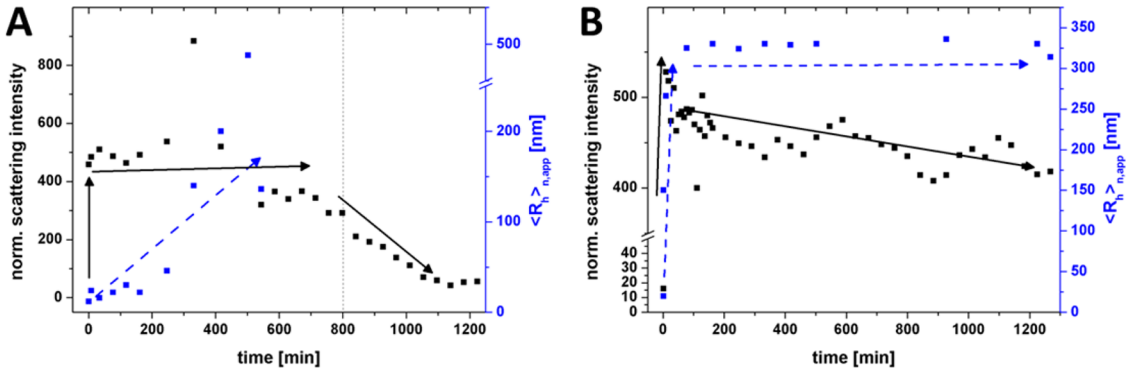

Figure 4. Normalized scattering intensity (black) and $\langle R_h \rangle_{n,app}$ (blue) over time, while the micellar solution was annealed at 65 °C (0.1 mg mL^{-1}) for PE_{36}-*b*-$PAmOx_{15}$-*b*-P*i*$PrOx_{145}$ (A) and PE_{36}-*b*-$PBocAmOx_{15}$-*b*-P*i*$PrOx_{145}$ (B).

P*i*PrOx upon crystallization within 10−12 h, while afterward the crystallization seems to "stop".[29−31,52] On the other hand, for PE_{36}-*b*-$PBocAmOx_{15}$-*b*-P*i*$PrOx_{145}$, the aggregate size increases within 2 h up to a plateau of ≈320 nm and no precipitation is observed. We assume partial crystallization of P*i*PrOx to be responsible for this phenomenon but are aware that a thorough variation of the corona length in such aggregates would be necessary to understand this behavior in detail. Similar behavior was observed for TB-$PAmOx_{15}$-*b*-P*i*$PrOx_{145}$, while in case of TB-$PBocAmOx_{15}$-*b*-P*i*$PrOx_{145}$, precipitation occurred within 10 h (Figure S19).

From DLS results, a clear difference between the aggregates formed *via* crystallization of P*i*PrOx for the two investigated triblock terpolymers can be deduced. Therefore, samples annealed for 24 h at 65 °C in water were investigated *via* transmission electron microscopy (TEM). Depending on the colloidal stability of the solution, TEM samples were prepared by direct

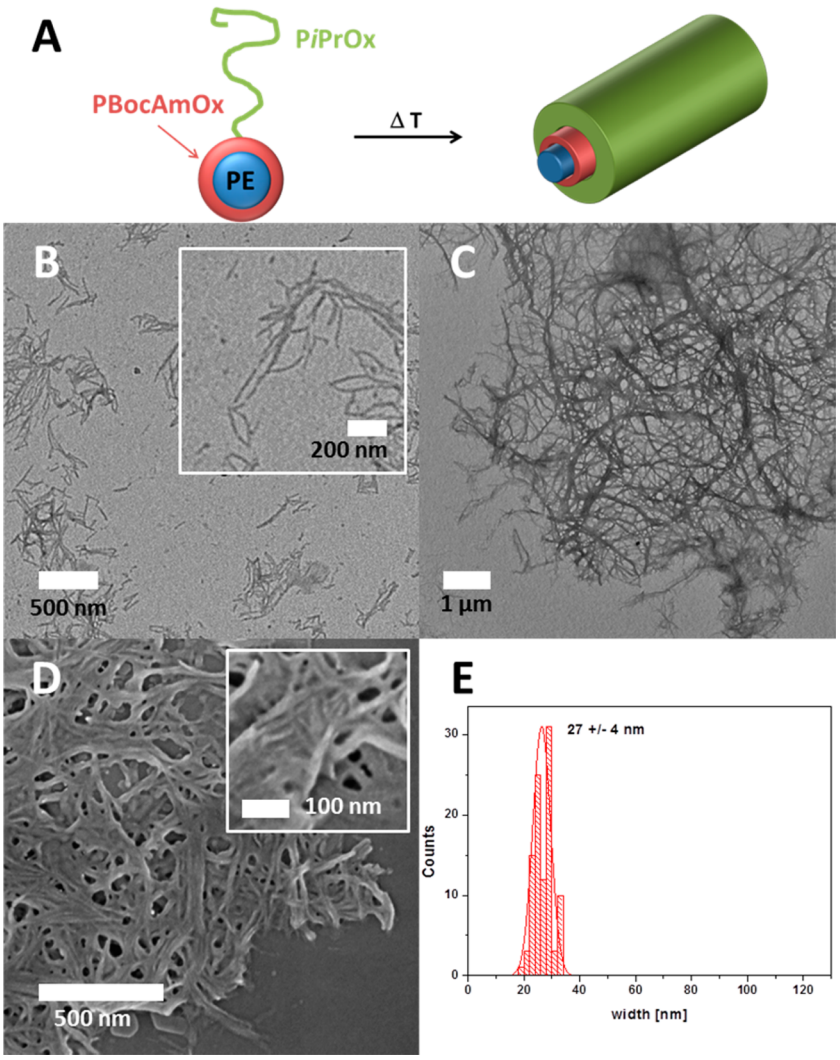

Figure 5. (A) Illustration of the aggregation mechanism of PE_{36}-*b*-$PBocAmOx_{15}$-*b*-$PiPrOx_{145}$ after directional crystallization of P*i*PrOx; (B and C) TEM micrographs of PE_{36}-*b*-$PBocAmOx_{15}$-*b*-$PiPrOx_{145}$ from aqueous solution after heating to 65 °C for 24 h; (D) SEM micrograph of PE_{36}-*b*-$PBocAmOx_{15}$-*b*-$PiPrOx_{145}$ from aqueous solution after heating to 65 °C for 24 h; (E) histogram of width distribution determined for cylindrical micelles as determined by grayscale analysis from TEM micrographs.

drop-casting from solution (PE_{36}-*b*-$PBocAmOx_{15}$-*b*-$PiPrOx_{145}$ and TB-$PAmOx_{15}$-*b*-$PiPrOx_{145}$) or by redispersing the precipitate (for PE_{36}-*b*-$PAmOx_{15}$-*b*-$PiPrOx_{145}$ and TB-$PBocAmOx_{15}$-*b*-$PiPrOx_{145}$) and subsequent drop-casting. In both cases, plasma treated carbon coated TEM grids were used.

For PE_{36}-*b*-$PBocAmOx_{15}$-*b*-$PiPrOx_{145}$, the material featuring the highest hydrophobic weight fraction, cylindrical micelles of several hundred nanometer length, also emanating from larger agglomerates (Figure 5B,C) were found by TEM and scanning electron microscopy (SEM; Figure 5D). The average width of the aggregates was determined by grayscale analysis of 100 individual cylinders, leading to 27 ± 4 nm (Figure 5E). Therefore, we assume a fusion of initially spherical micelles (R_h = 17 nm, diameter ~34 nm) upon heating. The annealing temperature of 65 °C is at the same time above the glass transition temperature (T_g) of PBocAmOx (≈ 40 °C)[49] and at the beginning of the melting range for PE (≈ 60 °C; observed *via* DSC Figure S7), thereby increasing chain mobility for both hydrophobic blocks. Crystallization of the P*i*PrOx corona then leads to unidirectional growth of the aggregates (Figure 5A).

While for PE_{36}-*b*-$PBocAmOx_{15}$-*b*-$PiPrOx_{145}$ the cylinder length of the micelles was rather short (50 nm −1000 nm) and mostly individual assemblies were found, PE_{36}-*b*-$PAmOx_{15}$-*b*-$PiPrOx_{145}$ formed long crystalline fibers of several micrometers in length (Figure 6B,C). Beside the fiber-like structures, "wool" like aggregates (darker areas observed by TEM; Figures S20 and S21) with diameters of 0.5−4 µm were found.[30] These structures were investigated by TEM and SEM and were found to match the aggregates described by Schlaad and co-workers. The formation is supposed to occur through secondary crystallization at the crystal interface (Figure 6D). These aggregates can be observed in all samples (PE_{36}-*b*-$PAmOx_{15}$-*b*-$PiPrOx_{145}$,

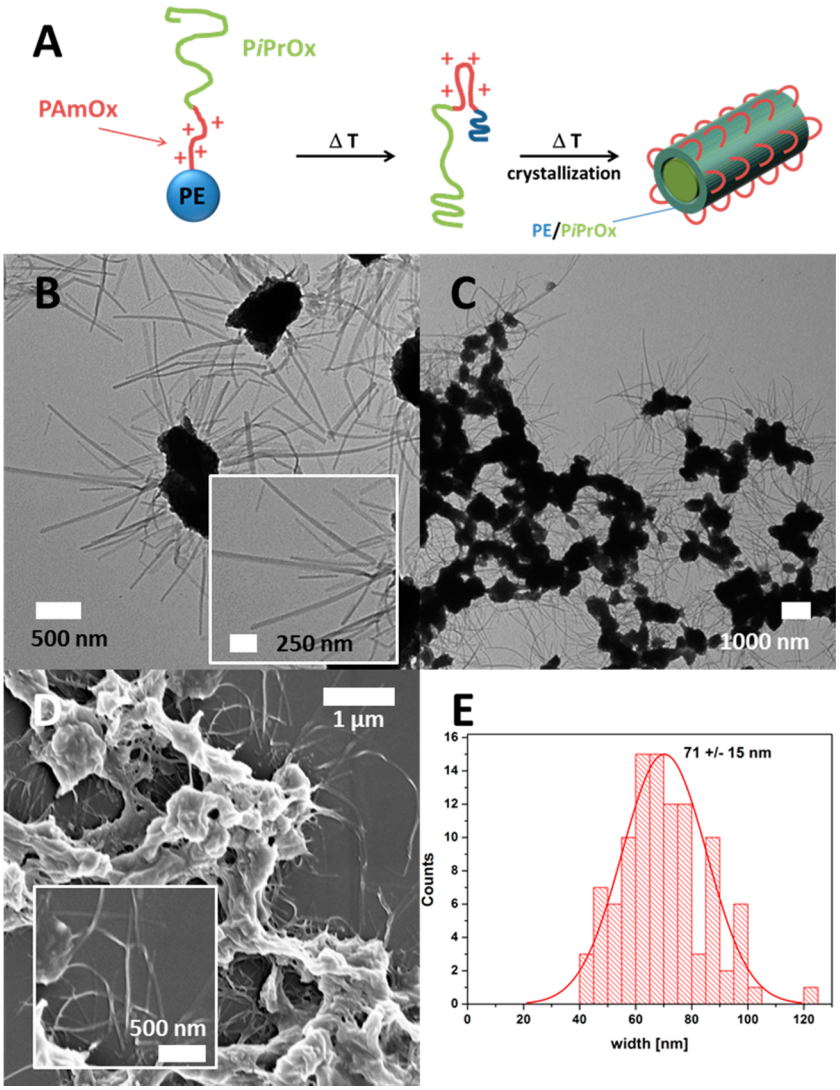

Figure 6. (A) Illustration of the proposed aggregation mechanism of PE_{36}-*b*-$PAmOx_{15}$-*b*-P*i*$PrOx_{145}$ after directional crystallization of P*i*PrOx; (B and C) TEM micrographs of PE_{36}-*b*-$PAmOx_{15}$-*b*-P*i*$PrOx_{145}$ from aqueous solution after heating to 65 °C for 24 h; (D) SEM micrograph of PE_{36}-*b*-$PAmOx_{15}$-*b*-P*i*$PrOx_{145}$ from aqueous solution after heating to 65 °C for 24 h; (E) histogram of width distribution determined for cylindrical micelles determined by grayscale analysis from TEM micrographs.

TB-$PBocAmOx_{15}$-*b*-P*i*$PrOx_{145}$, $PAmOx_{15}$-*b*-P*i*$PrOx_{145}$) and the overall quantity depends on the concentration.[30] Again, grayscale analysis was used to determine the width distribution for the cylinders, which was found to be 71 ± 15 nm and shows also greater variation along a single cylindrical aggregate (Figure 6D). Due to the differences observed in DLS and TEM, we assume a different mechanism for the crystallization of P*i*PrOx in this case. First, PE_{36}-*b*-$PAmOx_{15}$-*b*-P*i*$PrOx_{145}$ features a lower hydrophobic weight fraction (5 wt %) in comparison to PE_{36}-*b*-$PBocAmOx_{15}$-*b*-P*i*$PrOx_{145}$ (22 wt %) and second, the positively charged PAmOx segment might lead to an inversion of the core−shell−corona micelle at higher temperatures. The predicted corresponding pK_a value of the 4-aminobutyl moiety is around ≈10, and therefore, this segment is expected to be charged to a certain extent at pH 7.[54,55] In this case, upon heating above the LCST, P*i*PrOx forms the micellar core, partially incorporating the PE segment. PAmOx forms the corona, presumably as short loops (Figure 6A). Further heating then leads to crystallization of P*i*PrOx and the formation of cylindrical superstructures with a cationically charged outer layer.

To probe whether the pH value plays a significant role for the aggregation mechanism, PE_{36}-*b*-$PAmOx_{15}$-*b*-P*i*$PrOx_{145}$ was heated to 65 °C for 24 h at pH 12 resulting in aggregates with comparable size and shape as shown earlier at pH 7 (Figure S22). The width remains almost constant with 68 ± 19 nm (Figure S23). It seems that the increased hydrophilicity of the PAmOx block is sufficient to influence the aggregation mechanism even at pH-values where the amino group is not supposed to be significantly protonated.

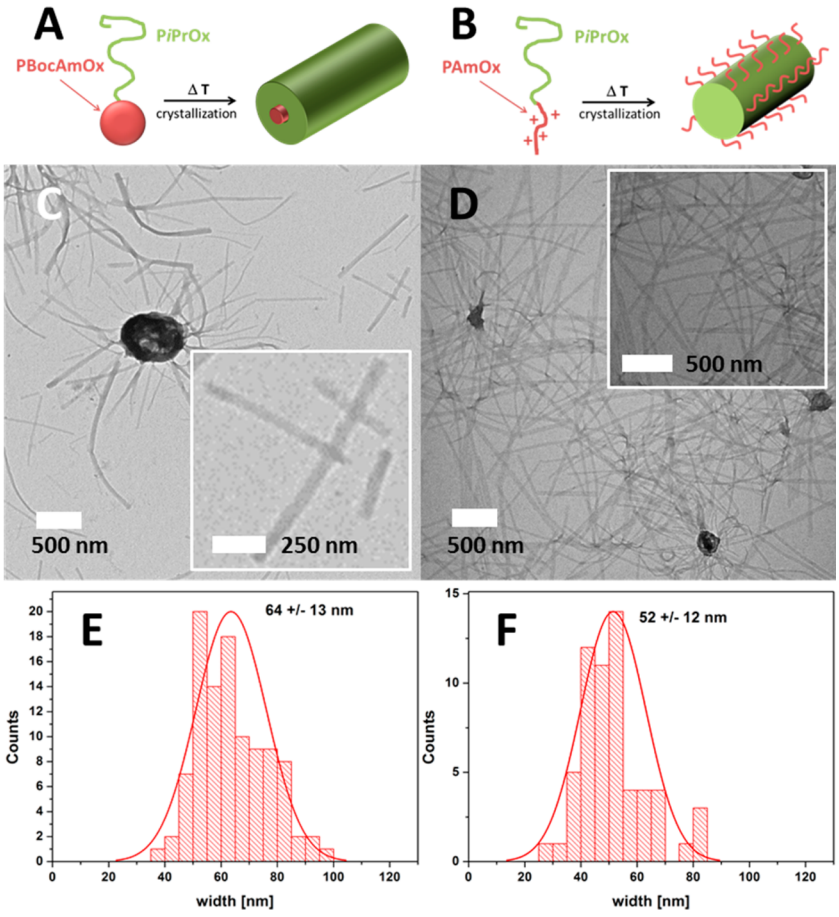

Figure 7. (A) Proposed aggregation mechanism of PBocAmOx$_{15}$-*b*-P*i*PrOx$_{145}$ after directional crystallization of P*i*PrOx; (B) proposed aggregation mechanism of PAmOx$_{15}$-*b*-P*i*PrOx$_{145}$ after directional crystallization of P*i*PrOx; (C) TEM micrograph of TB-PBocAmOx$_{15}$-*b*-P*i*PrOx$_{145}$ from aqueous solution after heating to 65 °C for 24 h; (D) TEM micrograph of PAmOx$_{15}$-*b*-P*i*PrOx$_{145}$ from aqueous solution after heating to 65 °C for 24 h; (E and F) histograms of width distribution determined for cylindrical micelles determined by grayscale analysis from TEM micrographs for PBocAmOx$_{15}$-*b*-P*i*PrOx$_{145}$ (E) and PBocAmOx$_{15}$-*b*-P*i*PrOx$_{145}$ (F).

For comparison, we also investigated the directional crystallization for both corresponding diblock copolymers, TB-PBocAmOx$_{15}$-*b*-P*i*PrOx$_{145}$ and TB-PAmOx$_{15}$-*b*-P*i*PrOx$_{145}$, under the same conditions. Whereas TB-PBocAmOx$_{15}$-*b*-P*i*PrOx$_{145}$ represents an amphiphilic material and a comparable aggregation mechanism can be assumed as discussed for PE$_{36}$-*b*-PAmOx$_{15}$-*b*-P*i*PrOx$_{145}$ earlier, in case of TB-PAmOx$_{15}$-*b*-P*i*PrOx$_{145}$, block copolymer unimers are initially present. In the latter case, directional crystallization of P*i*PrOx results in the formation of core–corona fibers with a polycationic outer layer (Figure 7A,B). The TEM micrographs show similar length and size distributions for the aggregates formed from TB-PBocAmOx$_{15}$-*b*-P*i*PrOx$_{145}$ and TB-PAmOx$_{15}$-*b*-P*i*PrOx$_{145}$. Grayscale analysis revealed diameters of 64 ± 13 and 52 ± 12 nm, respectively (Figure 7C–F; Table 2).

These observations, in our opinion, support the assumption of different crystallization mechanisms and highlight the importance of the PE block for the initial formation of well-defined core–shell–corona micelles building blocks.

TABLE 2. Characteristics for the Aggregates from Diblock Copolymers and Triblock Terpolymers Obtained by DLS before and TEM after Directional Crystallization of P*i*PrOx

polymer	hydrophilic part [wt %][a]	$\langle R_h \rangle_{n,app}$ [nm][b]	crystal width [nm][c]
TB-PAmOx$_{15}$-*b*-P*i*PrOx$_{145}$	100	2	52 ± 12
PE$_{36}$-*b*-PAmOx$_{15}$-*b*-P*i*PrOx$_{145}$	95	14	71 ± 15
TB-PBocAmOx$_{15}$-*b*-P*i*PrOx$_{145}$	82	13	64 ± 13
PE$_{36}$-*b*-PBocAmOx$_{15}$-*b*-P*i*PrOx$_{145}$	78	17	27 ± 4

[a] Calculated according to the block copolymer composition. [b] DLS, CONTIN plot; 25 °C before heating. [c] Average width size determined from TEM micrographs by grayscale analysis at 100 different positions after directional crystallization of P*i*PrOx.

To prove both the functionality of the presented materials and the existence of a partially cationic corona for primary amine containing superstructures, the incorporation of metal nanoparticles within the PAmOx part of the above-described anisotropic superstructures was investigated. For this purpose, we added either as-synthesized Fe_3O_4-nanocrystals with

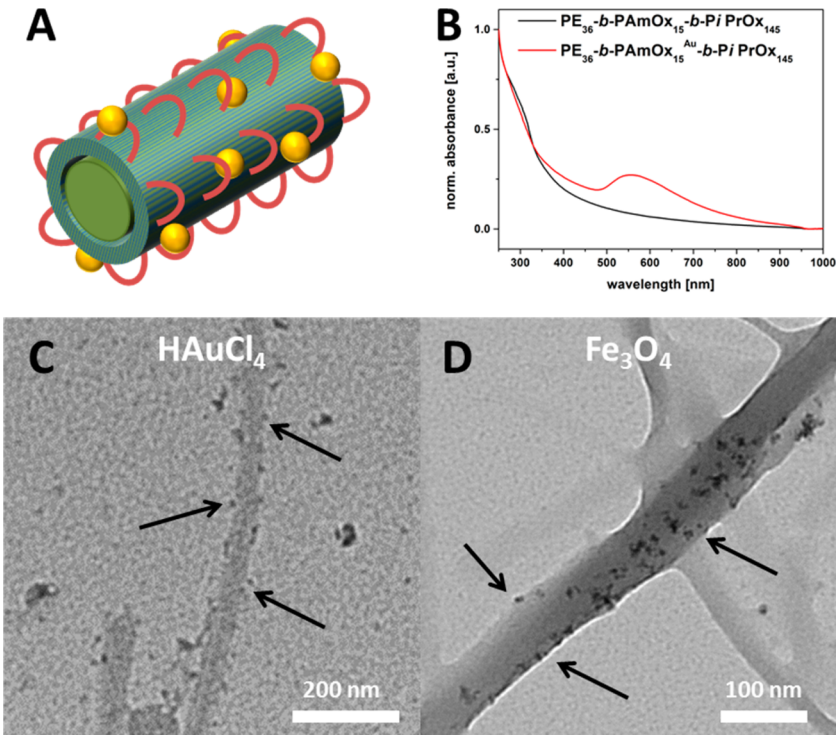

Figure 8. (A) Anisotropic hybrid cylinders of PE_{36}-*b*-$PAmOx_{15}$-*b*-P*i*$PrOx_{145}$ and metal nanoparticles; (B) comparison of UV−vis spectra for PE_{36}-*b*-$PAmOx_{15}$-*b*-P*i*$PrOx_{145}$ (black trace) and PE_{36}-*b*-$PAmOx_{15}^{Au}$-*b*-P*i*$PrOx_{145}$ (red trace); (C and D) TEM micrographs of PE_{36}-*click*-$PAmOx_{15}$-*b*-P*i*$PrOx_{145}$ fibers with (C) Au ions (reduced *in situ* by $NaBH_4$), (D) TEM micrograph of PE_{36}-*b*-$PAmOx_{15}$-*b*-P*i*$PrOx_{145}$ fiber-like micelles after the addition of Fe_3O_4 NPs (arrows indicate NP positions).

a diameter of 6 nm (obtained by an adopted literature protocol by pyrolyzing tris(acetylacetonato)iron(III) ($Fe(acac)_3$) in *N*-vinyl-2-pyrrolidone at 200 °C in the microwave, Figure S25)[56] or $HAuCl_4$ to micellar solutions of PE_{36}-*b*-$PAmOx_{15}$-*b*-P*i*$PrOx_{145}$ in water. After stirring for 12 h (in the dark in case of $HAuCl_4$), the solutions were dialyzed against water for 2 days. In case of $HAuCl_4$, 0.1 and 10 equiv of precursor/AmOx ratios (Au/AmOx) were tested. Afterward, heating for 24 h at 65 °C led to the formation of a precipitate as already discussed above. In case of $HAuCl_4$, subsequent reduction using sodium borohydride ($NaBH_4$) after the heating procedure resulted in the formation of Au NP. The hybrid structures from the coagulate were investigated by redispersing and drop-casting the solution onto TEM grids. As can be seen, anisotropic cylindrical superstructures were found in both cases. At higher magnification, increased attachment of the respective Au or Fe_3O_4 NPs to the fiber surface is visible. In case of Au NP, dark spots with a size of several nanometers can be found (Figure 8C; arrows indicate dark spots along the fiber; Figure S24). With the use of UV−vis spectroscopy, a slight absorption between 500 and 800 nm (absorbance maximum ≈555 nm) indicates the presence of Au NP (Figure 8B).[41,57] Similar results were observed if $HAuCl_4$ was reduced before or after the directional crystallization of P*i*PrOx. For the Fe_3O_4 nanocrystals, again preferential location within the outer layer of the anisotropic superstructures can be observed in TEM (Figure 8D; arrows guide the eye to NP positions; Figure S25).

In a further step, $HAuCl_4$ was also added to micellar solutions of PE_{36}-*b*-$PBocAmOx_{15}$-*b*-P*i*$PrOx_{145}$. After dialysis and directional crystallization, a weak signal could be detected in UV−vis, indicating the presence of Au NPs (Figure S27). However, these Au NPs according to TEM were randomly distributed (Figure S28), presumably due to the bulky protective groups shielding the amine moiety.

The position of either Au or Fe_3O_4 NPs confirms our hypothesis regarding the assembly mechanism of PE_{36}-*b*-$PAmOx_{15}$-*b*-P*i*$PrOx_{145}$ upon directional crystallization of P*i*PrOx. Both $HAuCl_4$ and the negatively charged Fe_3O_4 nanocrystals are attracted by a positively charged outer PAmOx layer.

CONCLUSION

We introduced a bottom-up strategy for the formation of anisotropic organic/inorganic hybrid fibers by directional crystallization of the poly(2-*iso*-propyl-2-oxazoline) (P*i*PrOx) corona of spherical core−shell−corona micelles in aqueous solution. For this purpose, we established the synthesis of a triblock terpolymer, polyethylene-*block*-poly(2-(4-(*tert*-butoxycarbonyl)-amino)butyl-2-oxazoline)-*block*-poly(2-*iso*-propyl-2-oxazoline) (PE_{36}-*b*-$PBocAmOx_{15}$-*b*-P*i*$PrOx_{145}$), by a combination of sequential polymerization and subsequent linkage by copper-catalyzed azide−alkyne

cycloaddition (CuAAC). Upon deprotection of the middle block to PAmOx primary, amine functionalities were generated. Due to the block sequence, the formation of spherical core−shell−corona micelles in solution was observed in both cases by DLS and TEM. In the next step, the directional crystallization of P*i*PrOx in water was investigated by heating the solution for 24 h to 65 °C. The crystallization was monitored *in situ* by DLS, while the resulting structures were investigated in detail by electron microscopy (TEM and SEM). Two different assembly mechanisms were identified for PE_{36}-*b*-$PBocAmOx_{15}$-*b*-P*i*$PrOx_{145}$ and PE_{36}-*b*-$PAmOx_{15}$-*b*-P*i*$PrOx_{145}$, presumably owing to differences in the hydrophobic weight fraction of 22 and 5 wt %, respectively. For PE_{36}-*b*-$PBocAmOx_{15}$-*b*-P*i*$PrOx_{145}$ (22 wt % hydrophobic), defined cylindrical micelles with a diameter of 27 nm were observed, while for the more hydrophilic PE_{36}-*b*-$PAmOx_{15}$-*b*-P*i*$PrOx_{145}$ (5 wt %), fiber-like structures of several micrometers in length and 60 nm width were formed. For PE_{36}-*b*-$PBocAmOx_{15}$-*b*-P*i*$PrOx_{145}$, we assume a fusion of initially spherical micelles into cylindrical superstructures, while in the case of PE_{36}-*b*-$PAmOx_{15}$-*b*-P*i*$PrOx_{145}$, P*i*PrOx, fibers with a positively charged PAmOx corona are formed. This was confirmed by the selective incorporation of Au and Fe_3O_4 nanoparticles within the AmOx corona. These first results toward the formation of anisotropic hybrid materials by linear triblock terpolymers with two crystalline segments demonstrate the potential of such materials for the controlled and stepwise directional assembly in solution into 2D or 3D structures. Optimization of corona length, loading efficiency, and length control for these systems will be the subject of further investigations.

EXPERIMENTAL SECTION

Instruments. *NMR.* Proton nuclear magnetic resonance (^{1}H NMR) spectra were recorded in $CDCl_3$ on a Bruker AC 300 MHz spectrometer at 298 K. Chemical shifts are given in parts per million (ppm, δ scale) relative to the residual signal of the deuterated solvent.

For PE samples, NMR spectroscopy was carried out with a Bruker DRX 400 spectrometer operating at 400 MHz. Spectra were recorded at 363 K using a 5 mm QNP probe for ^{1}H NMR. Polymer samples were examined as 5−15% (w/v) solutions. A mixture of tetrachloroethylene (TCE) and deuterated benzene (C_6D_6) (2/1 v/v) was used as solvent. Chemical shift values are given in units of ppm, relative to an internal reference of tetramethylsilane for ^{1}H.

SEC. Size exclusion chromatography was measured on a Shimadzu system equipped with a SCL-10A system controller, a LC-10AD pump, a RID-10A refractive index detector, and both a PSS Gram30 and a PSS Gram1000 column in series, whereby *N*,*N*-dimethylacetamide (DMAC) with 5 mmol of LiCl was used as an eluent at 1 mL min^{-1} flow rate and the column oven was set to 60 °C. The system was calibrated with PS (100 to 1 000 000 g mol^{-1}) standards. Furthermore, a Shimadzu system equipped with an SCL-10A system controller, an LC-10AD pump, and an RID-10A refractive index detector using a solvent mixture containing chloroform ($CHCl_3$), triethylamine (TEA), and *iso*-propyl alcohol (*i*-PrOH) (94:4:2) at a flow rate of 1 mL min^{-1} on a PSS SDV linear M 5 μm column at 40 °C was used. The system was calibrated using polystyrene (100 to 100 000 g mol^{-1}) standards.

High Temperature SEC. High temperature size exclusion chromatography (HT-SEC) analyses were performed using a Viscotek system (from Malvern Instruments) equipped with three columns (PLgel Olexis 300 mm × 7 mm i.d. from Agilent Technologies). A volume of 200 μL of sample solutions with concentration of 5 mg mL^{-1} was eluted in 1,2,4-trichlorobenzene (TCB) using a flow rate of 1 mL min^{-1} at 150 °C. The mobile phase was stabilized with 2,6-di(*tert*-butyl)-4-methylphenol (200 mg L^{-1}). The OmniSEC software was used for data acquisition and data analysis. The molar mass distributions were calculated with a calibration curve based on narrow polyethylene standards (M_p: 170, 395, 750, 1110, 2155, 25 000, 77 500, 126 000 g mol^{-1}) from Polymer Standard Service (Mainz).

FT-IR Infrared Spectroscopy. Dry powders of the materials were directly placed on the crystal of the ATR-FTIR (Affinity-1 FTIR, Shimadzu) for measurements in the range of 4000 to 600 cm^{-1}.

Microwave-Assisted Polymerizations. These were carried out utilizing an Initiator Sixty single-mode microwave synthesizer from Biotage, equipped with a noninvasive IR sensor (accuracy: 2%). Microwave vials (conical, 0.5−2 mL) were heated at 110 °C overnight and allowed to cool to room temperature under nitrogen atmosphere. All polymerizations were carried out using temperature control.

DLS. Dynamic light scattering was performed at a scattering angle of 90° on an ALV CGS-3 instrument equipped with a He−Ne laser operating at a wavelength of 633 nm at 25 °C. Micelle solutions were filtered before measurement (Nylon; 0.45 μm). The CONTIN algorithm was applied to analyze the obtained correlation functions. For temperature control, the DLS is equipped with a Lauda thermostat. Apparent hydrodynamic radii were calculated according to the Stokes−Einstein equation.

Transmission Electron Microscopy. The formed aggregates were analyzed using a TEM (Zeiss-CEM 902A, Oberkochen, Germany) operated at 80 kV. Images were recorded using a 1k TVIPS FastScan CCD camera or on a FEI Tecnai G^2 20 (200 kV, operated at 120 kV) equipped with a 4k × 4k Eagle HS CCD and a 1k × 1k Olympus MegaView camera for overview images. TEM samples were prepared by applying a drop of an aqueous sample solution onto the surface of a plasma-treated carbon coated copper grid (Quantifoil Micro-Tools GmbH, Jena, Germany).

Scanning Electron microscopy. Zeiss SIGMA VP Field Emission SEM equipped with the GEMINI column (Carl-Zeiss AG, Germany) operating at 3−7 kV using the InLens or SE2 detector.

Materials. Propargyl *p*-toluenesulfonate and 2-*iso*-propyl-2-oxazoline (*i*PrOx) were distilled over barium oxide under vacuum and stored under nitrogen atmosphere in a glovebox. 2-(4-(*tert*-Butoxycarbonyl)amino)butyl-2-oxazoline (BocAmOx) was synthesized according to literature reports[49] and distilled prior to usage and stored in a glovebox. Tetrahydrofuran (THF), acetonitrile (CH_3CN), and dichloromethane (CH_2Cl_2) were purified using a Solvent Purification System (SPS, Innovative Technology, PM-400-3-MD) equipped with two activated alumina columns. Copper bromide (CuBr) and *N*,*N*,*N*′,*N*″,*N*″-pentamethyldiethylenetriamine (PMDETA) were purchased from Aldrich and used as received. If not mentioned otherwise, the educts were used as received. For ethylene polymerization: catalyst $(C_5Me_5)_2NdCl_2Li(OEt_2)_2$ synthesis was carried out under an argon atmosphere using standard Schlenk techniques, according to a literature procedure.[58] Polymerization was carried out in a glass reactor under anoxic, aprotic conditions, with ethylene (N35, Air Liquide) supplied *via* a 2.13 L ballast chamber to monitor consumption. Toluene and tetrahydrofuran were degassed by argon passage and purified with an SPS800 MBraun solvent purification system. All other chemicals were used as supplied: cocatalyst butyloctylmagnesium solution in

heptane (0.88 M, Chemtura), iodine (ACS reagent, ≥ 99.8%, solid, Sigma-Aldrich), sodium azide (≥99%, solid, Sigma-Aldrich), *N*,*N*-dimethylformamide (HLPC grade, Biosolve).

Synthesis. *Synthesis of Iodo End-Functionalized Polyethylene (PE−I).* The polymerization was carried out in a glass reactor under anoxic, aprotic conditions, with ethylene supplied *via* a 2.13 L ballast chamber to monitor consumption. A solution of *n*-butyloctylmagnesium in heptane (0.88 mol L^{-1}) was diluted with toluene (400 mL). The resulting solution was transferred to a reactor under an argon atmosphere. An antechamber was then charged with a suspension of $(C_5Me_5)_2NdCl_2Li(OEt_2)_2$ ([Mg]/[Nd] = 150) in toluene (10 mL). The reactor was heated to 75 °C and then charged with an ethylene atmosphere at a pressure of 3 bar. The precatalyst suspension was then added to the reactor and the consumption of ethylene monitored. When the desired amount of ethylene was consumed, the ethylene atmosphere was replaced with argon. The reactor contents were cooled to 10 °C and a solution of iodine ([I]/[Mg] = 4) in THF (50 mL) was added and the suspension stirred for 1 h. The reactor contents was precipitated into methanol (200 mL) and the suspension was filtered. The solid recovered was washed three times with methanol (3 × 100 mL) and dried.

SEC (TCB/150 °C): M_n = 1260 g mol^{-1}; Đ = 1.17. NMR (400 MHz; TCE/C_6D_6): 2.94 (t, $-CH_2I$), 1.66 (q, CH_2CH_2I), 1.24 (b, $CH_2CH_2)_n$, 0.83 (t, $-CH_2CH_3$). Functionalization: 87% (calculated from ^{1}H NMR).

Synthesis of Azide End-Functionalized Polyethylene (PE−N_3) from PE−I. A solution of 5 g of PE−I in a mixture of toluene/DMF (2/1) containing 1.2 equiv of sodium azide was degassed under argon and then heated to 120 °C. After 2 h, the reaction mixture was slowly cooled to room temperature and was poured in methanol. The solid recovered was filtered off, washed three times with methanol (3 × 100 mL), and dried under vacuum.

SEC (TCB/150 °C): M_n = 1290 g mol^{-1}; Đ = 1.16. NMR (400 MHz; TCE/C_6D_6): 2.99−2.96 ($-CH_2N_3$), 1.42−1.37 ($-CH_2CH_2N_3$), 1.24 (b, $CH_2CH_2)_n$, 0.83 (t, $-CH_2CH_3$). Functionalization: 87% (calculated from ^{1}H NMR).

Synthesis of Alkyne-Modified Poly(2-(4-(tert-butoxycarbonyl)-amino)butyl-2-oxazoline)-block-Poly(2-iso-propyl-2-oxazoline) Block Copolymer (PBocAmOx$_{15}$-b-PiPrOx$_{145}$). Propargyl *p*-toluenesulfonate and 2-(4-(*tert*-butoxycarbonyl)-amino)butyl-2-oxazoline (BocAmOx) were dissolved in acetonitrile (CH_3CN), a monomer to initiator ratios of 15 and a monomer concentration of 1 mol L^{-1}. The capped vial was placed in a microwave synthesizer at 140 °C. After the polymerization, the vial was transferred into a glovebox. A stock solution of 2-*iso*-propyl-2-oxazoline and CH_3CN (1 mol L^{-1}) were added to the polymer solution. The capped vial was and placed in the microwave synthesizer at 140 °C again to form the block copolymer. A small amount of the first block was kept under inert atmosphere at room temperature and was investigated together with the other polymers *via* SEC and NMR. The block copolymers were terminated *via* the addition of water, and removing the solvent under reduced pressure.

SEC ($CHCl_3$/TEA/*i*-PrOH): M_n = 23 500 g mol^{-1}; Đ = 1.08. SEC (DMAC/LiCl): M_n = 28 000 g mol^{-1}; Đ = 1.09. NMR (300 MHz; $CDCl_3$): 5.5−4.8 (−NH), 3.9−3.1 (backbone), 3.1−3.0 ($-CH_2$-Boc), 3.0−2.5 ($-CO-CH_2-^{iPrOx}$), 2.5−2.2 ($-CO-CH_2-^{BocAmOx}$), 1.75−1.5 ($-CH_2-CH_2-^{BocAmOx}$), 1.42 ($-CH_3^{BocAmOx}$), 1.2−0.7 ($-CH_3^{iPrOx}$) ppm. FT-IR: 3300 (−NH), 1705 ($C{=}O^{Boc}$), 1630 ($C{=}O^{POx}$), 1516 (amide), 1365 ($-CH_3^{Boc}$) cm^{-1}.

Synthesis of Triblock Terpolymers via CuAAC between the Azide-Modified PE$_{36}$−N_3 and Diblock Copolymers (PE$_{36}$-b-PBocAmOx$_{15}$-b-PiPrOx$_{145}$). A total of 100 mg (6 μmol) of the diblock copolymer was dissolved together with 20 mg of PE$_{36}$−N_3 (16.4 μmol; 2.73 equiv) and copper bromide (CuBr; 2 equiv) in tetrahydrofuran (THF) at 120 °C in a sealed pressure vial. Obtaining a clear solution, *N*,*N*,*N*′,*N*″,*N*″-pentamethyldiethylenetriamine (PMDETA; 2 equiv) was added under stirring. The solution was stirred at 120 °C for 1 h and subsequently cooled to room temperature and diluted with water. The turbid solution was filtered and washed with acetone. The aqueous solution was vigorously stirred with dichloromethane (CH_2Cl_2). The clear organic phase was filtered with a syringe filter (PTFE; 0.45 μm), twice, and dried under vacuum. The obtained polymer was precipitated in cold diethyl ether, filtered, and dried under vacuum.

SEC ($CHCl_3$/TEA/*i*-PrOH): M_n = 24 000 g mol^{-1}; Đ = 1.09. SEC (DMAC/LiCl): M_n = 27 000 g mol^{-1}; Đ = 1.11. ^{1}H NMR (300 MHz; $CDCl_3$): 5.5−4.8 (−NH), 3.9−3.1 (backbone), 3.2−3.0 ($-CH_2$-Boc), 3.0−2.5 ($-CO-CH_2-^{iPrOx}$), 2.5−2.2 ($-CO-CH_2-^{BocAmOx}$), 1.75−1.5 ($-CH_2-CH_2-^{BocAmOx}$), 1.42 ($-CH_3^{BocAmOx}$), 1.25 (PE backbone), 1.3−0.7 ($-CH_3^{iPrOx}$) ppm. FT-IR: 3070−2785 ($-CH_2-$), 1701 ($C{=}O^{Boc}$), 1630 ($C{=}O^{POx}$), 1514 (amide), 1365 ($-CH_3^{Boc}$) cm^{-1}.

Deprotection of Triblock Terpolymers PE$_{36}$-b-PBocAmOx$_{15}$-b-PiPrOx$_{145}$. The triblock terpolymer PE$_{36}$-*click*-PBocAmOx$_{15}$-*b*-PiPrOx$_{145}$ (80 mg; 4 μmol) was dissolved in trifluoroacetic acid (TFA, 2 mL, 26 mmol), stirred for 1 h at 60 °C and for 20 h at room temperature. The solution was diluted with methanol (2 mL) and precipitated in cold diethyl ether (150 mL, −80 °C). The polymer was filtered off and dissolved in a mixture of methanol and chloroform (1/1, 200 mL), and subsequently stirred with Amberlyst A21 for 3 days. After filtration, the solvents were evaporated and the product was dried under high vacuum.

SEC (DMAC/LiCl): M_n = 25 000 g mol^{-1}; Đ = 1.06. NMR (300 MHz; $CDCl_3$): 3.9−3.1 (backbone), 3.0−2.5 ($-CO-CH_2-^{iPrOx}$), 2.0−1.5 ($-CH_2-CH_2-^{AmOx}$), 1.25 (PE backbone), 1.2−0.7 ($-CH_3^{iPrOx}$) ppm. FT-IR: 3070−2785 ($-CH_2-$), 1630 ($C{=}O^{POx}$) 1162, 824, 800, 717 (amine) cm^{-1}.

Synthesis of Alkyne-Modified Poly(2-(4-(amino)butyl)-2-oxazoline)-block-Poly(2-iso-propyl-2-oxazoline) Block Copolymer (TB-PAmOx$_{15}$-b-PiPrOx$_{145}$). The diblock copolymer TB-PBocAmOx$_{15}$-*b*-PiPrOx$_{145}$ (80 mg; 4 μmol) was dissolved in trifluoroacetic acid (TFA, 2 mL, 26 mmol), stirred for 1 h at 60 °C and for 20 h at room temperature. The solution was diluted with methanol (2 mL) and precipitated in cold diethyl ether (150 mL, −80 °C). The polymer was filtered off and dissolved in a mixture of methanol and chloroform (1/1, 200 mL), and subsequently stirred with Amberlyst A21 for 3 days. After filtration, the solvents were evaporated and the product was dried under high vacuum.

SEC (DMAC/LiCl): M_n = 29 000 g mol^{-1}; Đ = 1.07. NMR (300 MHz; $CDCl_3$): 3.9−3.1 (backbone), 3.0−2.5 ($-CO-CH_2-^{iPrOx}$), 2.0−1.5 ($-CH_2-CH_2-^{AmOx}$), 1.2−0.7 ($-CH_3^{iPrOx}$) ppm. FT-IR: 3070−2785 ($-CH_2-$), 1630 ($C{=}O^{POx}$) 1150, 824, 800, 717 (amine) cm^{-1}.

Synthesis of Fe_3O_4 Nanocrystals[56]. For the preparation of Fe_3O_4 nanocrystals, tris(acetylacetonato)iron(III) ($(Fe(acac)_3$); 283 mg, 0.8 mmol) was dissolved in 2 mL of *N*-vinyl-2-pyrrolidon (NVP) in a microwave vial and heated to 200 °C for 20 min under microwave irradiation. The mixture was diluted with deionized water (300 mL) and centrifuged at 11 000 rpm for 15 min. The washing procedure was repeated until the supernatant of the nanocrystals remained colorless.

Self-Assembly of Triblock Terpolymers in Aqueous Media. Ten milligrams of the respective triblock terpolymer was dissolved in 10 mL of DMF (1 mg mL^{-1}) and heated in an oil bath to 120 °C for 10 min under stirring. Afterward, the solution was allowed to cool down to room temperature. The solution was dialyzed against water for 2 days (RC, MWCO 1000).

Incorporation of Nanoparticles in PE$_{36}$-click-PAmOx$_{15}$-b-PiPrOx$_{145}$. Ten milligrams of the respective triblock terpolymer were dissolved in 10 mL of DMF (1 mg mL^{-1}) and heated in an oil bath to 120 °C for 10 min under stirring; afterward, the solution was allowed to cool to room temperature. One milliliter of a stock solution of $HAuCl_4$ (1 mg mL^{-1}) or Fe_3O_4 nanocrystals (1 mg mL^{-1}) was added to the micellar solution at room temperature. Afterward, the solutions were stirred for 12 h (in the dark in case of added $HAuCl_4$), and subsequently dialyzed against water for 2 days (RC, MWCO 1000; in the dark in case of gold precursor), before the solutions were heated up for 24 h at 65 °C. In case of the gold precursor solution, the dialysis bag turned red due to the reduction of uncomplexed gold salt. For the reduction of the complexed gold precursor, sodium borohydride ($NaBH_4$) was added to the solution, which turned slightly red.

Conflict of Interest: The authors declare no competing financial interest.

Acknowledgment. The authors thank Stefanie Rudolph for help with the grayscale analysis of TEM micrographs, Christian Pietsch for SEM measurements, Grit Festag for SEC measurements, and Stephanie Hoeppener for help with TEM analysis. The TEM facilities were funded by a grant of the DFG and EFRE (European Fund for Regional Development). F.H.S. and T.R. are further grateful to the Thuringian Ministry for Education, Science, and Culture (TMBWK; #B515-10065, ChaPoNano; #B515-11028, SWAXS-JCSM) for financial support. F.H.S. thanks the VCI for a starting independent researcher fellowship. T.R. acknowledges the Carl-Zeiss foundation for a Ph.D. scholarship.

Supporting Information Available: The Supporting Information is available free of charge on the ACS Publications website at DOI: 10.1021/acsnano.5b03660.

Additional experimantal data (PDF)

REFERENCES AND NOTES

1. Bates, F. S.; Fredrickson, G. H. Block Copolymer-Designer Soft Materials. *Phys. Today* **1999**, *52*, 32–38.
2. Mai, Y.; Eisenberg, A. Self-Assembly of Block Copolymers. *Chem. Soc. Rev.* **2012**, *41*, 5969–5985.
3. Abetz, V.; Simon, P., *Phase Behaviour and Morphologies of Block Copolymers (Block Copolymers I)*; Abetz, V., Ed.; Springer: Berlin/Heidelberg, 2005; Vol. 189, pp 125−212.
4. Schacher, F. H.; Rupar, P. A.; Manners, I. Functional Block Copolymers: Nanostructured Materials with Emerging Applications. *Angew. Chem., Int. Ed.* **2012**, *51*, 7898–7921.
5. Xi, W.; Scott, T. F.; Kloxin, C. J.; Bowman, C. N. Click Chemistry in Materials Science. *Adv. Funct. Mater.* **2014**, *24*, 2572–2590.
6. Kolb, H. C.; Finn, M. G.; Sharpless, K. B. Click Chemistry: Diverse Chemical Function from a Few Good Reactions. *Angew. Chem., Int. Ed.* **2001**, *40*, 2004–2021.
7. Iha, R. K.; Wooley, K. L.; Nyström, A. M.; Burke, D. J.; Kade, M. J.; Hawker, C. J. Applications of Orthogonal "Click" Chemistries in the Synthesis of Functional Soft Materials. *Chem. Rev.* **2009**, *109*, 5620–5686.
8. Kempe, K.; Krieg, A.; Becer, C. R.; Schubert, U. S. ″Clicking″ on/with Polymers: a Rapidly Expanding Field for the Straightforward Preparation of Novel Macromolecular Architectures. *Chem. Soc. Rev.* **2012**, *41*, 176–191.
9. Liang, L.; Astruc, D. The Copper(I)-Catalyzed Alkyne-Azide Cycloaddition (CuAAC) "Click" Reaction and its Applications: an Overview. *Coord. Chem. Rev.* **2011**, *255*, 2933–2945.
10. Binder, W. H.; Sachsenhofer, R. 'Click' Chemistry in Polymer and Materials Science. *Macromol. Rapid Commun.* **2007**, *28*, 15–54.
11. Espeel, P.; Du Prez, F. E. Click"-Inspired Chemistry in Macromolecular Science: Matching Recent Progress and User Expectations. *Macromolecules* **2015**, *48*, 2–14.
12. Barner-Kowollik, C.; Du Prez, F. E.; Espeel, P.; Hawker, C. J.; Junkers, T.; Schlaad, H.; Van Camp, W. Clicking" Polymers or Just Efficient Linking: What Is the Difference? *Angew. Chem., Int. Ed.* **2011**, *50*, 60–62.
13. Lang, C.; Voll, D.; Inglis, A. J.; Dingenouts, N.; Goldmann, A. S.; Barner, L.; Barner-Kowollik, C. An Access Route to Polyferrocenes *via* Modular Conjugation. *Macromol. Chem. Phys.* **2011**, *212*, 831–839.
14. Altintas, O.; Rudolph, T.; Barner-Kowollik, C. Single Chain Self-Assembly of Well-Defined Heterotelechelic Polymers Generated by ATRP and Click Chemistry Revisited. *J. Polym. Sci., Part A: Polym. Chem.* **2011**, *49*, 2566–2576.
15. Rudolph, T.; Nunns, A.; Schwenke, A. M.; Schacher, F. H. Synthesis and Self-Assembly of Poly(ferrocenyldimethylsilane)-*block*-poly(2-alkyl-2-oxazoline) Block Copolymers. *Polym. Chem.* **2015**, *6*, 1604–1612.
16. Zhang, M.; Rupar, P. A.; Feng, C.; Lin, K.; Lunn, D. J.; Oliver, A.; Nunns, A.; Whittell, G. R.; Manners, I.; Winnik, M. A. Modular Synthesis of Polyferrocenylsilane Block Copolymers by Cu-Catalyzed Alkyne/Azide "Click" Reactions. *Macromolecules* **2013**, *46*, 1296–1304.
17. Fournier, D.; Hoogenboom, R.; Schubert, U. S. Clicking Polymers: a Straightforward Approach to Novel Macromolecular Architectures. *Chem. Soc. Rev.* **2007**, *36*, 1369–1380.
18. Hanisch, A.; Schmalz, H.; Müller, A. H. E. A Modular Route for the Synthesis of ABC Miktoarm Star Terpolymers *via* a New Alkyne-Substituted Diphenylethylene Derivative. *Macromolecules* **2012**, *45*, 8300–8309.
19. Rudolph, T.; Crotty, S.; Lühe, M. v. d.; Pretzel, D.; Schubert, U. S.; Schacher, F. H. Synthesis and Solution Properties of Double Hydrophilic Poly(ethylene oxide)-*block*-poly(2-ethyl-2-oxazoline) (PEO-*b*-PEtOx) Star Block Copolymers. *Polymers* **2013**, *5*, 1081–1101.
20. Altintas, O.; Vogt, A. P.; Barner-Kowollik, C.; Tunca, U. Constructing Star Polymers *via* Modular Ligation Strategies. *Polym. Chem.* **2012**, *3*, 34–45.
21. Durmaz, H.; Sanyal, A.; Hizal, G.; Tunca, U. Double Click Reaction Strategies for Polymer Conjugation and Post-Functionalization of Polymers. *Polym. Chem.* **2012**, *3*, 825–835.
22. Wang, X.; Guerin, G.; Wang, H.; Wang, Y.; Manners, I.; Winnik, M. A. Cylindrical Block Copolymer Micelles and Comicelles of Controlled Length and Architecture. *Science* **2007**, *317*, 644–7.
23. Gädt, T.; Ieong, N. S.; Cambridge, G.; Winnik, M. A.; Manners, I. Complex and Hierarchical Micelle Architectures from Diblock Copolymers Using Living, Crystallization-Driven Polymerizations. *Nat. Mater.* **2009**, *8*, 144–150.
24. Gilroy, J. B.; Gädt, T.; Whittell, G. R.; Chabanne, L.; Mitchels, J. M.; Richardson, R. M.; Winnik, M. A.; Manners, I. Monodisperse Cylindrical Micelles by Crystallization-Driven Living Self-Assembly. *Nat. Chem.* **2010**, *2*, 566–570.
25. Massey, J. A.; Temple, K.; Cao, L.; Rharbi, Y.; Raez, J.; Winnik, M. A.; Manners, I. Self-Assembly of Organometallic Block Copolymers: The Role of Crystallinity of the Core-Forming Polyferrocene Block in the Micellar Morphologies Formed by Poly(ferrocenylsilane-*b*-dimethylsiloxane) in *n*-Alkane Solvent. *J. Am. Chem. Soc.* **2000**, *122*, 11577–11584.
26. Schmelz, J.; Schedl, A. E.; Steinlein, C.; Manners, I.; Schmalz, H. Length Control and Block-Type Architectures in Worm-Like Micelles with Polyethylene Cores. *J. Am. Chem. Soc.* **2012**, *134*, 14217–25.
27. Schmelz, J.; Schacher, F. H.; Schmalz, H. Cylindrical Crystalline-Core Micelles: Pushing the Limits of Solution Self-Assembly. *Soft Matter* **2013**, *9*, 2101.
28. Qiu, H.; Hudson, Z. M.; Winnik, M. a.; Manners, I. Multidimensional Hierarchical Self-Assembly of Amphiphilic Cylindrical Block Comicelles. *Science* **2015**, *347*, 1329–1332.
29. Demirel, A. L.; Meyer, M.; Schlaad, H. Formation of Polyamide Nanofibers by Directional Crystallization in Aqueous Solution. *Angew. Chem., Int. Ed.* **2007**, *46*, 8622–8624.
30. Diehl, C.; Cernoch, P.; Zenke, I.; Runge, H.; Pitschke, R.; Hartmann, J.; Tiersch, B.; Schlaad, H. Mechanistic Study of the Phase Separation/Crystallization Process of Poly(2-*iso*-propyl-2-oxazoline) in Hot Water. *Soft Matter* **2010**, *6*, 3784–3788.
31. Meyer, M.; Antonietti, M.; Schlaad, H. Unexpected Thermal Characteristics of Aqueous Solutions of Poly(2-*iso*-propyl-2-oxazoline). *Soft Matter* **2007**, *3*, 430–431.
32. Katsumoto, Y.; Tsuchiizu, A.; Qiu, X.; Winnik, F. M. Dissecting the Mechanism of the Heat-Induced Phase Separation and Crystallization of Poly(2-*iso*-propyl-2-oxazoline) in Water through Vibrational Spectroscopy and Molecular Orbital Calculations. *Macromolecules* **2012**, *45*, 3531–3541.
33. Guillerm, B.; Monge, S.; Lapinte, V.; Robin, J. J. How to Modulate the Chemical Structure of Polyoxazolines by Appropriate Functionalization. *Macromol. Rapid Commun.* **2012**, *33*, 1600–1612.
34. Mathew, B.; Pillai, V. N. R. Polymer-Metal Complexes of Amino Functionalized Divinylbenzene-Crosslinked Polyacrylamides. *Polymer* **1993**, *34*, 2650–2658.
35. Nicolaus, V.; Wöhrle, D. Synthesis and Transition Metal Complex Binding of Amines and Amides Covalently Bound to Crosslinked Polystyrene. *Angew. Makromol. Chem.* **1992**, *198*, 179–190.

36. Förster, S.; Antonietti, M. Amphiphilic Block Copolymers in Structure-Controlled Nanomaterial Hybrids. *Adv. Mater.* **1998**, *10*, 195–217.
37. Yuan, J.; Xu, Y.; Müller, A. H. E. One-Dimensional Magnetic Inorganic-Organic Hybrid Nanomaterials. *Chem. Soc. Rev.* **2011**, *40*, 640–655.
38. Sanchez, C.; Julian, B.; Belleville, P.; Popall, M. Applications of Hybrid Organic-Inorganic Nanocomposites. *J. Mater. Chem.* **2005**, *15*, 3559–3592.
39. Schacher, F. H.; Rudolph, T.; Drechsler, M.; Müller, A. H. E. Core-Crosslinked Compartmentalized Cylinders. *Nanoscale* **2011**, *3*, 288–297.
40. Rivas, B. L.; Pereira, E. D.; Moreno-Villoslada, I. Water-Soluble Polymer-Metal Ion Interactions. *Prog. Polym. Sci.* **2003**, *28*, 173–208.
41. Kretschmer, F.; Mansfeld, U.; Hoeppener, S.; Hager, M.; Schubert, U. S. Tunable Synthesis of Poly(ethylene imine)-Gold-Nanoparticle Clusters. *Chem. Commun.* **2014**, *50*, 88–90.
42. Lu, Y.; Mei, Y.; Schrinner, M.; Ballauff, M.; Möller, M. W.; Breu, J. *In Situ* Formation of Ag Nanoparticles in Spherical Polyacrylic Acid Brushes by UV Irradiation. *J. Phys. Chem. C* **2007**, *111*, 7676–7681.
43. Lu, W.; Lieber, C. M. Nanoelectronics from the Bottom Up. *Nat. Mater.* **2007**, *6*, 841–850.
44. Katz, E.; Willner, I. Integrated Nanoparticle-Biomolecule Hybrid Systems: Synthesis, Properties, and Applications. *Angew. Chem., Int. Ed.* **2004**, *43*, 6042–108.
45. Cheng, M. M.; Cuda, G.; Bunimovich, Y. L.; Gaspari, M.; Heath, J. R.; Hill, H. D.; Mirkin, C. A.; Nijdam, A. J.; Terracciano, R.; Thundat, T.; Ferrari, M. Nanotechnologies for Biomolecular Detection and Medical Diagnostics. *Curr. Opin. Chem. Biol.* **2006**, *10*, 11–19.
46. Briquel, R.; Mazzolini, J.; Le Bris, T.; Boyron, O.; Boisson, F.; Delolme, F.; D'Agosto, F.; Boisson, C.; Spitz, R. Polyethylene Building Blocks by Catalyzed Chain Growth and Efficient End Functionalization Strategies, Including Click Chemistry. *Angew. Chem., Int. Ed.* **2008**, *47*, 9311–9313.
47. D'Agosto, F.; Boisson, C. A RAFT Analogue Olefin Polymerization Technique Using Coordination Chemistry. *Aust. J. Chem.* **2010**, *63*, 1155–1158.
48. Valente, A.; Mortreux, A.; Visseaux, M.; Zinck, P. Coordinative Chain Transfer Polymerization. *Chem. Rev.* **2013**, *113*, 3836–3857.
49. Hartlieb, M.; Pretzel, D.; Kempe, K.; Fritzsche, C.; Paulus, R. M.; Gottschaldt, M.; Schubert, U. S. Cationic Poly(2-oxazoline) Hydrogels for Reversible DNA Binding. *Soft Matter* **2013**, *9*, 4693.
50. Bieligmeyer, M.; Taheri, S. M.; German, I.; Boisson, C.; Probst, C.; Milius, W.; Altstadt, V.; Breu, J.; Schmidt, H. W.; D'Agosto, F.; Förster, S. Completely Miscible Polyethylene Nanocomposites. *J. Am. Chem. Soc.* **2012**, *134*, 18157–60.
51. Oleszko, N.; Utrata-Wesołek, A.; Wałach, W.; Libera, M.; Hercog, A.; Szeluga, U.; Domański, M.; Trzebicka, B.; Dworak, A. Crystallization of Poly(2-*iso*-propyl-2-oxazoline) in Organic Solutions. *Macromolecules* **2015**, *48*, 1852–1859.
52. Hoogenboom, R.; Schlaad, H. Bioinspired Poly(2-oxazoline)s. *Polymers* **2011**, *3*, 467–488.
53. Rudolph, T.; Nunns, A.; Stumpf, S.; Pietsch, C.; Schacher, F. H. Hierarchical Self-Assembly of Double-Crystalline Poly(ferrocenyldimethylsilane)-*block*-poly(2-*iso*-propyl-2-oxazoline) (PFDMS-*b*-PiPrOx) Block Copolymers. *Macromol. Rapid Commun.* **2015**, 10.1002/marc.201500245.
54. Hall, H. K. Correlation of the Base Strengths of Amines. *J. Am. Chem. Soc.* **1957**, *79*, 5441–5444.
55. Geurts, J. M.; Göttgens, C. M.; Graefschepe, M. A. I. V.; Welland, R. W. A.; Es, J. J. G. S. V.; German, A. L. Syntheses of New Amino-Functionalized Methacrylates and Their Use in Free Radical Polymerizations. *J. Appl. Polym. Sci.* **2001**, *80*, 1401–1415.
56. Lu, X.; Niu, M.; Qiao, R.; Gao, M. Superdispersible PVP-Coated Fe_3O_4 Nanocrystals Prepared by a "One-Pot" Reaction. *J. Phys. Chem. B* **2008**, *112*, 14390–14394.
57. Hoerenz, C.; Rudolph, T.; Barthel, M. J.; Guenther, U.; Schacher, F. H. Amphiphilic Polyether-Based Block Copolymers as Crosslinkable Ligands for Au-Nanoparticles. *Polym. Chem.* **2015**, *6*, 5633–5642.
58. Tilley, T. D.; Andersen, R. A. Pentamethylcyclopentadienyl Derivatives of the Trivalent Lanthanide Elements Neodymium, Samarium, and Ytterbium. *Inorg. Chem.* **1981**, *20*, 3267–3270.